Research Article | Vol. 27, No. 6 | 18 Mar 2019 | OPTICS EXPRESS 8168
Optics EXPRESS

Single-channel bimodal interferometric sensor using subwavelength structures

L. TORRIJOS-MORÁN AND J. GARCÍA-RUPÉREZ*

Nanophotonics Technology Center, Universitat Politècnica de València, Camino de Vera s/n, 46022 Valencia, Spain
jaigarru@ntc.upv.es

Abstract: A novel configuration of photonic sensors based on a single-channel bimodal interferometer is proposed. The design consists of a subwavelength grating (SWG) periodic structure supporting two dispersive TE-like modes that interfere at the output to create fringes in the transmission spectrum. Dispersion relations of the bimodal periodic structures have been computed in order to study the sensing performance, obtaining a theoretical bulk sensitivity of ~1300nm/RIU and a surface sensitivity of ~6.1nm/nm. Finite-Difference Time Domain (FDTD) analysis has been also carried out in order to confirm the previously obtained sensitivity results, thus showing a perfect agreement between theoretical modelling and simulation.

© 2019 Optical Society of America under the terms of the OSA Open Access Publishing Agreement

1. Introduction

Electromagnetic wave propagation through periodic dielectric media has been widely studied in the literature for a huge range of configurations and applications, among which we can find periodic structures for sensing purposes [1,2]. Within this field, the most relevant examples are photonic crystals (PhCs), which consist of a periodic dielectric repetition in the space for one, two or three dimensions. They were firstly described in detail in [3] as a powerful tool for the implementation of all kind of photonic devices, being later used for a wide range of applications such as modulators, delay lines or filters [4,5]. Various types of photonic crystals have been also demonstrated for sensing applications [6–8], offering several advantages in terms of sensitivity and compactness as a consequence of their inherent dispersion properties.

More recently, other type of periodic structures have emerged as a promising alternative in the biosensors field: the so-called subwavelength grating (SWG) structures. These structures can be considered as uniaxial PhCs with lower periodicity values so that the light propagates through the structure as if it were a homogeneous medium, in comparison to the Bragg's behavior occurring in PhCs [9]. Moreover, for periodicity values lower than the wavelength of light, the refractive index (RI) of the resultant metamaterial can be engineered to create photonic devices with enhanced properties. This is the case of broadband beam splitters based on a SWG structure where dispersion control was used [10,11], tilted structures controlling anisotropy [12] or high-performance ring resonator (RR) sensors whose sensitivity is around three times that of a conventional RR sensor [13].When a cladding RI variation takes place, the effective index change of a SWG waveguide mode is significantly higher than for a normal strip waveguide due to the interaction of not only the evanescent field but also the field of the propagating mode itself [14,15]. This fact has given rise to the appearance of new photonic sensors based on SWG configurations, offering remarkable advantages respect to the old existing ones and opening new opportunities in this area.

At the same time, integrated interferometers have been commonly used as sensors in lab-on-a-chip (LoC) devices during the last years, with great advantages in terms of sensitivity for label-free detection [16]. Among them, Mach Zehnder Interferometer (MZI) is the most representative configuration [17,18] although it needs from additional structures like MMIs or power splitters to perform the sensing. In addition, different approaches have been reported in

#355279 https://doi.org/10.1364/OE.27.008168
Journal © 2019 Received 13 Dec 2018; revised 29 Jan 2019; accepted 3 Feb 2019; published 6 Mar 2019

Optics EXPRESS

the study of interferometric sensors with enhanced sensitivities in spectral interrogation-based sensing [19]. A MZI with different waveguide widths between both arms was experimentally demonstrated for this effect in [20], reporting really high bulk sensitivity values as a consequence of the differential phase shift between the excited modes. On the other hand, single-channel interferometer sensors such as bimodal waveguides appear as one of the best options for integration purposes in LoC devices due to their simplicity and outstanding surface sensitivity for biosensing [21–25]. The sensing principle of these sensors is based on the phase shift produced between the two first TE modes propagating through a bimodal waveguide and measured at the output by a photodetector. However, long bimodal sections are required in order to achieve enough phase shift sensitivity as it scales with sensor length, leading to large footprints of several millimeters or even centimeters.

In this paper, we report the design of a new modal sensor by using a SWG waveguide as a single-channel interferometer. This concept encompasses the benefits of SWG structures in terms of high sensitivity to effective indices variations, while maintaining the characteristics and benefits of bimodal interferometric waveguides. Moreover, as a consequence of working with periodic structures, dispersive modes can be obtained for the SWG structure while behaving like a homogenous medium, what also introduces some of the advantages of PhCs for sensing. As a result, a differential phase shift providing an extremely high spectral sensitivity is obtained, without the need of large paths and additional photonic structures. Band diagrams of the two first TE-like modes were computed to obtain the differential phase shift between them, as well as FDTD simulations to check the spectral response of the sensor under different sensing scenarios, showing bulk sensitivities around 1300nm/RIU and surface sensitivities of 6.1 nm/nm. This work expands the use of SWG structures for interferometric sensing purposes, exhibiting high sensitivities and allowing its integration in reduced footprints of only few microns.

2. Operation theory

When an object structure is larger than the wavelength of light, its electromagnetic behavior can be modelled by the Snell's law using reflection, diffraction and refraction coefficients. Wave propagation through a periodic repetition of this kind of structures gives rise to a lossy system where no light is guided as a consequence of scattering effects [26]. Conversely, if we consider a periodic medium whose lattice constant is much smaller than wavelength, light propagates through the structure as if it were a homogenous medium where diffraction effects are suppressed, thereby obtaining a SWG configuration. Between these two regimes, when the periodicity is not small enough to avoid diffraction, rigorous solution of Maxwell's electromagnetic equations is needed to describe the optical properties of the resultant structure: a PhC. The most common way to delimit these regions and to determine whether we are working in the SWG regime or not is described by the expression $\lambda/\Lambda>2n_{eff}$ where λ is the operating wavelength and Λ is the periodicity value [27].

Here, we work with periods close to the SWG limit and near the PhC zone, where the periodic structure supports two true lossless modes as a consequence of working in the subwavelength regime but with some of the dispersion properties typical of periodic structures. This fact generates non-linear phase shifts falls between both modes that cannot be obtained with a normal bimodal waveguide. The design of the proposed sensor is presented in Fig. 1. It is composed by a SWG bimodal section with a width enough to support two guided TE-like modes with different symmetry in the 'x' axis (even and odd) for the wavelength range of interest. By properly placing the single mode waveguide used as input port, both modes of the SWG section are excited. After propagating through the bimodal section, these two modes will interfere and contribute to the excitation of the fundamental mode of the single mode waveguide used as output port. The output power will therefore depend on the phase shift between both modes, creating constructive or destructive interferences when the differential phase is an even or an odd multiple of π, respectively. These interferences will

Optics EXPRESS

give rise to the appearance of spectral dips in the transmission spectrum for those wavelengths where the modes interfere destructively.

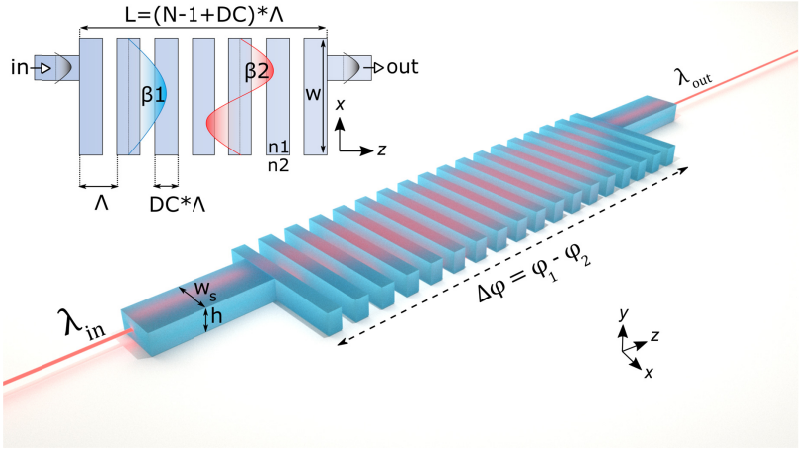

Fig. 1. Schematic representation of the proposed SWG bimodal sensor where 'Λ' is the period, 'DC' the duty cycle of the SWG elements, 'w' the width of the SWG elements, 'h' the height and 'w_s' the width of the input and output waveguides. The length '*L*' is determined by the number of elements N: L = (N-1 + DC)*Λ. The inset schematically shows the profile of the propagating modes.

The wavevector difference between the SWG modes for a given cladding RI can be expressed as $\Delta k_{n1} = k_1 - k_2$ where $k_{1,2}$ are the wavevectors in the propagation direction of the even and odd modes, respectively. When a RI variation is produced in the cladding of the SWG sensing structure, the differential phase shift between both modes is described by the following equation:

$$\Delta\varphi = L\left|\delta k_1 - \delta k_2\right|, \tag{1}$$

where L is the length of the SWG bimodal section and $\delta k_{1,2}$ are the wavevectors differential for a small change in the cladding RI. Taking into account the dispersion properties of the guided modes, non-linear phase shifts as a function of wavelength are obtained. Consequences of this effect are studied by calculating the dispersion diagrams of the periodic structures and how they behave for changes of the cladding RI. In the following sections, we study how to benefit from dispersion effects in a bimodal SWG interferometric structure to enhance the spectral sensitivity.

3. Sensitivity analysis

3.1 Bulk sensing

In spectral interrogation based sensors such as resonators, the sensitivity is measured from the spectral shift suffered by the spectral features of interest when a change in the refractive index of the cladding is produced [28]. This type of sensors can define its bulk sensitivity as [29]:

$$S_b = \frac{\delta\lambda_f}{\delta n_c}, \tag{2}$$

where $\delta\lambda_f$ expresses the shift in nm of a spectral feature for a differential change in the cladding RI δn_c measured in refractive index units (RIU). In this type of spectral interrogation based sensors, it has been demonstrated both theoretically and experimentally that significantly higher spectral shifts are obtained when using SWG structures, since a dramatic change in the modes propagation constant is produced [13]. These sensing benefits of SWG-

Optics EXPRESS

based sensors do not only lie in a stronger mode delocalization, but mainly in the direct interaction of the optical field with the target medium in the gaps of the SWG elements.

By multiplying and dividing the expression in Eq. (2) by $\delta\varphi$, we obtain an analytical expression for the bulk sensitivity as a function of the phase shift between the even and odd modes of the SWG bimodal sensor:

$$S_b = \frac{\delta\varphi / \delta n_c}{\delta\varphi / \delta\lambda_f}. \tag{3}$$

As it can be seen, the sensitivity is inversely proportional to the phase derivative with respect to the wavelength. Because of this, the bulk sensitivity can be analytically infinite as long as the slope of the phase as a function of wavelength reaches zero. This critical lambda point appears for those values where $\delta\varphi/\delta\lambda_f = 0$, as it is reported in [19], and consequently, higher sensitivities are achieved as we get closer to this working point.

Several simulations using MIT Photonics Band (MPB) free software have been carried out in order to obtain the electromagnetic modes of the periodic SWG sensing structure and their dispersion relations. This software computes definite-frequency eigenstates of Maxwell's equations in fully-vectorial and three-dimensional spaces, calculating dispersion relations of the periodic structures for different wavevector points [30]. We have considered a SWG structure made of silicon (n = 3.47) over a silica substrate (n = 1.44) and an aqueous environment as upper cladding (n≈1.36), for which two TE-like modes are supported for an operation wavelength around 1550nm when the design values are Λ = 290nm, DC = 50%, w = 1400nm and h = 220nm. Due to scaling properties of periodic configurations, the bimodal region can be shifted to other operating wavelengths by properly selecting the period of the structure. The band diagrams obtained for the even and odd TE-like modes of this SWG structure are shown in Fig. 2(a), while Fig. 2(b) shows the phase shift between these two modes as a function of wavelength for different cladding RIs.

The first thing we can highlight from Fig. 2(b) is that the sign of the wavelength shift changes from positive to negative values as we move towards higher wavelengths, obtaining a zero-sensitivity point between these two regions for which the phase remains the same regardless the RI of the cladding. We can also observe that an abrupt fall in the phase shift with respect to the wavelength is produced for lower wavelengths, what is determined by the highly dispersive behavior of the even and odd modes near the edge of the Brillouin zone, as shown in Fig. 2(a). Contrary for higher wavelengths, the group velocity of the odd mode increases and starts becoming non-dispersive, provoking a change in the trend of the phase shift and therefore to the appearance of lower slopes as a function of wavelength. Taking into account this fact, the maximum sensitivity appears for the spectral fringes located in the critical sensitivity zone, which is defined as the highest wavelength spectral region where the bimodal condition is obtained, in which the phase slope is close to zero, as it was determined in Eq. (3). Note that, for even higher wavelengths, the odd mode goes below the light cone of the silica lower cladding and becomes a leaky mode, so this spectral region is not considered for the operation of the SWG bimodal interferometer sensor. Finally, we can also highlight that the odd mode presents a lower effective index than the even mode, thus having a higher interaction with the surrounding medium since it is less confined.

Optics EXPRESS

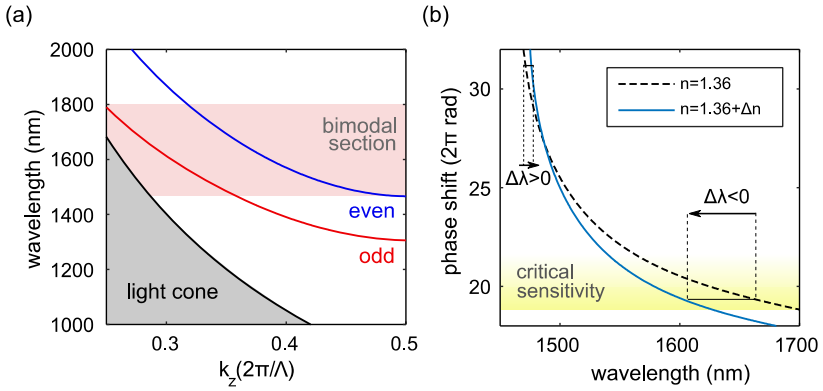

Fig. 2. (a) Dispersion relations of the even and odd TE-like modes of a SWG bimodal structure of period Λ = 290nm, DC = 50%, w = 1400nm and h = 220nm, under an aqueous environment as cladding (n = 1.36). (b) Phase shift as a function of wavelength between both modes for a cladding of 1.36RIU and for a RI change of Δn = 0.07RIU; N = 40 periods have been considered.

The influence of the duty cycle over the phase shift is depicted in Fig. 3(a) under an aqueous environment of 1.36RIU and when a RI increment of 0.01RIU is considered. It can be seen how the wavelength shift increases with the duty cycle due to the reduction of the slope of the phase shift as a function of wavelength for higher duty cycles. However, additional propagating modes might be supported by the SWG structure when the duty cycle is increased, thus losing the bimodal condition required for the operation of the interferometric sensor. In addition, critical sensitivity regions are narrower for higher duty cycles, making it more difficult to design spectral dips at those zones. Therefore, a trade-off is produced between sensitivity and proper operation, obtaining good results for average values of the duty cycle.

Figure 3(b) depicts the sensitivity curves for the different duty cycles considered in the study. They have been numerically calculated from the MPB band diagrams by obtaining the absolute value of the wavelength shift between both modes when considering cladding RI variations being multiple of 3.3×10^{-3}RIU. An operating wavelength of $\lambda = 1665$nm has been considered to calculate the sensitivity, since it is within the critical sensitivity range and close to the light cone for the considered design. Bulk sensitivity values of 778.28nm/RIU, 1065.1nm/RIU and 1202.9nm/RIU have been numerically obtained for duty cycles of 40%, 50% and 60%, respectively. In comparison with the literature, a sensitivity of 490nm/RIU was experimentally obtained using a SWG RR [13]. This sensitivity value was recently enhanced by using a multi-box SWG RR, presenting bulk sensitivities of 580nm/RIU [31]. Therefore, our proposed sensor configuration theoretically shows bulk sensitivities more than twice of that reported for other spectral interrogation based SWG sensors, what represents a significant step forward within this type of structures. Note that similar sensitivities to those calculated for our bimodal SWG sensor have been also obtained for other configurations, as for example when using slot waveguide RRs [32]. However, the fabrication of this type of structures is significantly more challenging than for the relatively simple bimodal SWG configuration proposed in this work.

Additionally, semi-analytical bulk sensitivities have been also calculated using Eq. (3) by applying finite differential derivatives, with respect to the cladding RI and the wavelength, on the phase shifts obtained in MPB. A comparison between the numerical and semi-analytical results are presented in Fig. 3(c), showing a good agreement for the different duty cycles considered. However, the difference between numerical and semi-analytical results increase with the duty cycle, obtaining a sensitivity as high as 1298nm/RIU for the semi-analytical study in the case of a DC of 60%.

Optics EXPRESS

Finally, it should be noted that the bulk wavelength sensitivity does not directly depend on the sensor length if we are measuring the spectral shift. By increasing the sensor length, we can increase the number of fringes appearing at the same spectral range, but the wavelength shift of each spectral feature will remain the same.

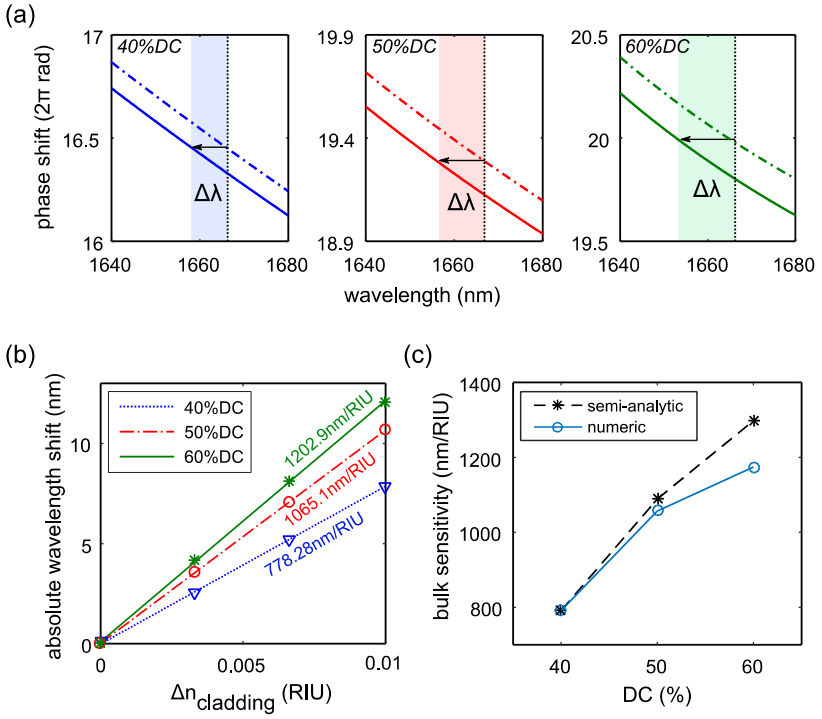

Fig. 3. (a) Phase shift between both modes of the SWG bimodal structure for different duty cycles. Dashed and solid lines show the phase shift for a cladding RI of 1.36RIU and 1.37RIU, respectively. Design parameters are Λ = 290nm, DC = 50%, w = 1400nm and h = 220nm. (b) Numerical wavelength shift as a function of the cladding RI for different duty cycles at 1665nm. Note that the spectral features located in the critical sensitivity region are shifted towards lower wavelengths for increments of the cladding RI, so absolute values of the wavelength shift are considered. (c) Bulk sensitivity comparison between the numerical and the semi-analytic calculations obtained using Eq. (3) at an operation wavelength of 1665nm.

3.2 Surface sensing

The surface sensitivity relates the shift of a given spectral feature with the thickness of a certain layer with a different RI than the cladding, considering what happens when a certain biological substance is deposited over the sensor. In the literature, it is defined in nm/nm by the following expression for spectral interrogation based sensors [33]:

$$S_s = \frac{\Delta\lambda_f}{\rho_{layer}}, \tag{4}$$

where $\Delta\lambda_f$ is the feature spectral shift and ρ_{layer} is the thickness of the deposited layer. The surface sensitivity has been numerically calculated using MPB for several thicknesses of a layer deposited over the SWG sensing structure and considering an operation in the critical sensitivity region. Figure 4(a) shows the surface sensitivity results obtained for different duty cycles as a function of the layer thickness, while Fig. 4(b) depicts the surface sensitivity as a function of the wavelength for a SWG structure of 60% duty cycle when the thickness of the deposited layer increases from 10nm to 100nm. Note that since high wavelength shifts of the bimodal region are obtained when different layers are considered, we cannot obtain a

Optics EXPRESS

common operating wavelength for all thicknesses. Therefore, we have considered as operating wavelengths those where maximum surface sensitivity values are placed. Hence, in order to obtain the maximum surface sensitivity results as possible in future designs, the operating wavelength will depend on the thickness of the specific biolayer to be detected.

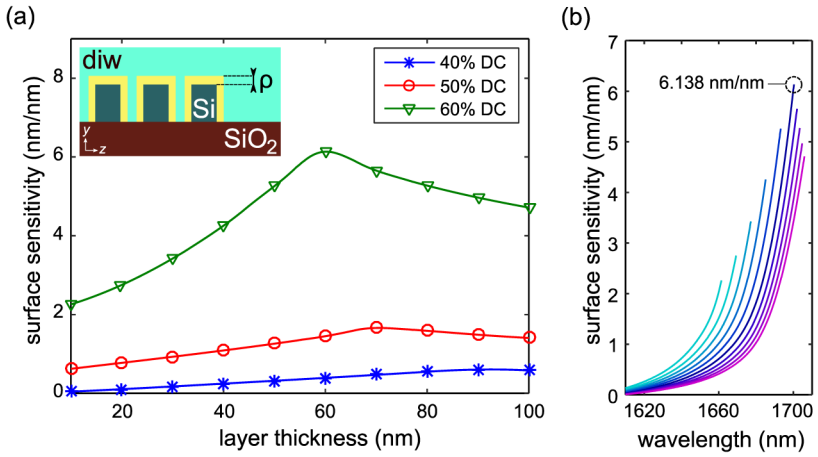

Fig. 4. (a) Surface sensitivity as a function of the layer thickness ρ for the SWG bimodal sensor in an aqueous environment for different duty cycles. The inset depicts the cross section of the transversal SWG elements in the y-z plane with the deposited layer. A RI of 1.48RIU is considered for the deposited layer. (b) Surface sensitivity as a function of wavelength for different layer thicknesses and a duty cycle of 60%. The layer thickness goes from 10nm (light blue) to 100nm (purple). Note that sensitivity values have been calculated considering only wavevectors for which the modes remain above the light cone of the silica lower cladding.

A maximum surface sensitivity of 6.138nm/nm has been obtained for a layer thickness of 60nm in the case of 60%DC. As it was explained before, results are strongly dependent on the duty cycle, considerably enhancing the surface sensitivity by a factor higher than three in the case of 60% compared to the case of 50%. This is due to the significant reduction of the phase slope obtained for duty cycles above 50%, as it was previously shown in Fig. 3(a). On the other hand, surface sensitivity decays for certain thicknesses due to the overlap of the deposited layer within the gap of the SWG elements. These outstanding results are obtained thanks to the direct interaction of the optical modes with the deposited layer, obtaining maximum sensitivity values when the hole is totally filled with the target substance. Such big layers around 60-70nm could be interesting in biosensing applications, for example, in the recognition of viruses or other biological substance with similar dimensions. Nonetheless, the detection of small protein layers of few nanometers is still feasible using this sensor, since more than 2nm/nm of surface sensitivity is obtained for a thickness of 10nm, making it a promising configuration for biosensing purposes.

Revising the literature, surface sensitivity values around 0.4nm/nm have been previously presented for a conventional RR sensor working for TM polarization; these values have been recently increased until 1nm/nm and 2nm/nm for a SWG RR and for a multi-box SWG RR, respectively, all of them for small layer thicknesses around 10nm [34]. Our results show better surface sensitivities for this thicknesses range when considering a 60% duty cycle and an ultrahigh sensitivity behavior for layers around 60nm, compared to the values below 0.5nm/nm reported in the multi-box SWG RR for thicker layers.

Optics EXPRESS

4. Spectral analysis

4.1 SWG bimodal sensor excitation

FDTD simulations have been carried out using CST Studio software with the aim of analyzing the sensor response when it is excited using the single mode access waveguides. In order to properly excite both modes, an asymmetric coupling of the single mode waveguide in the x axis is needed. The field distribution of the even and odd modes of the SWG structure, calculated by using RSOFT software, is depicted in Fig. 5(a) as well as the profiles of the modes in Fig. 5(b). It can be seen that both modes are confined inside the silicon elements of the SWG structure in the case of the x component of the electric field. However, high values of the z component distribution are located within the gaps, what explains the strong field interaction with the cladding. From Fig. 5(b) we can observe that the x-axis of the even mode is strongly localized in the center of the SWG structure, while the odd mode is distributed on its outer sides. So, in order to properly excite both modes, the single mode access waveguide has to be displaced respect to the center of the SWG structure (x = 0 position). Figure 5(c) shows the transmission spectra calculated for a SWG bimodal sensor with a duty cycle of 50% when different lateral positions of an access waveguide of width w_s = 450nm are considered (centered access waveguide - d = 700nm / displaced access waveguide - d = 375nm). An interference fringe can be observed in the spectrum for the displaced waveguide excitation, while an almost flat spectrum is obtained when the single mode waveguide is centered since only the even mode is excited. Finally, note that the number of spectral dips available can be significantly increased by simply increasing the length of the SWG bimodal sensor since higher phase shifts are then reached for the same range of wavelengths.

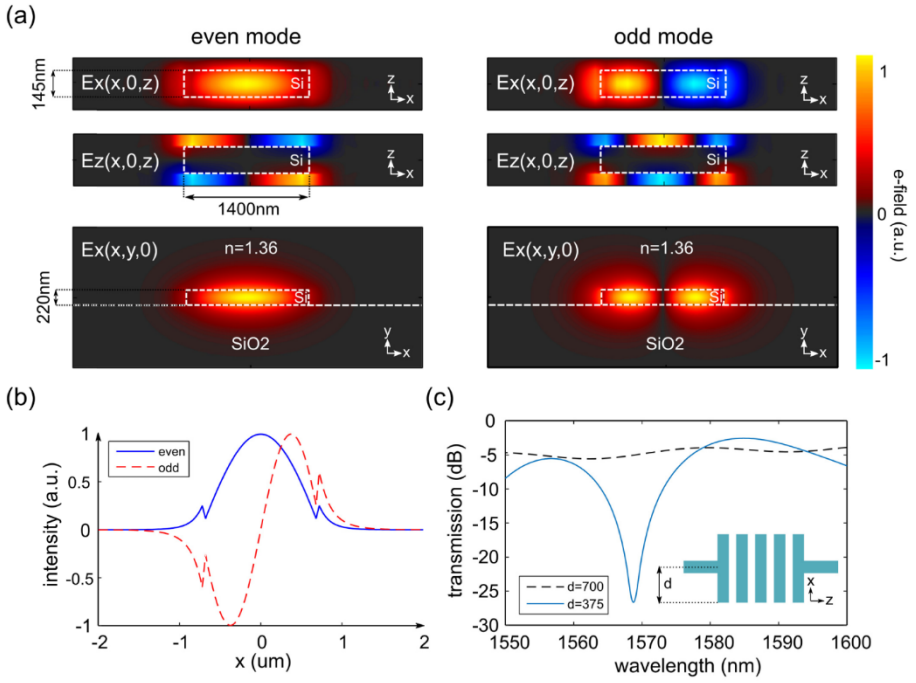

Fig. 5. (a) Electric field magnitude distribution of a periodic cell of the SWG structure in different planes for even and odd modes. The white dashed rectangles represent the SWG element. Design parameters are Λ = 290nm, DC = 50%, w = 1400nm and h = 220nm for a silica lower cladding and an aqueous environment of 1.36RIU. (b) Mode profile of the x-component of the electric field for both modes in the x-axis at y = 0 and z = 0. (c) Transmission spectra for a 50% duty cycle SWG bimodal structure as a function of the

Optics EXPRESS

displacement 'd' of a single mode waveguide of width w_s = 450nm at the input and output. A length of N = 120 elements has been considered for the calculations.

4.2 Spectral sensing response

The transmission spectrum of the SWG bimodal sensor has been obtained using FDTD simulations when considering different RI claddings, in order to study the sensing characteristics of the final device. As it was previously seen, bulk sensitivity depends on wavelength since the phase shift between the SWG modes shows a non-linear behavior and it reaches an almost zero slope for higher wavelengths within the bimodal bandwidth. Therefore, an accurate design of the sensor is key to obtain optimum spectral dips at critical sensitivity wavelengths to take maximum advantage from the sensor. Making the sensor longer produces more spectral features in the bimodal region, easing the design of high sensitivity fringes. However, when the cladding RI changes, so does the fringe wavelength and consequently its sensing performance.

Figure 6(a) shows the sensor behavior of the higher wavelength spectral feature appearing in the spectrum for two different duty cycles (see Fig. 6(b)). The SWG structures have been designed in order to obtain that spectral feature around 1665nm with the purpose of being able to compare the FDTD results with those previously obtained using MPB. In order to locate the spectral feature at that wavelength, we have simply properly selected the number of transversal elements considered in the SWG bimodal structure (N of 120 and 220 for duty cycles of 50% and 60%, respectively). Sensitivities of 1070.1nm/RIU and 1375.5nm/RIU have been obtained for duty cycles of 50% and 60%, respectively. Additionally, Fig. 6(c) depicts the x-component of the electric field distribution in FDTD at operating wavelengths corresponding to constructive and destructive interferences.

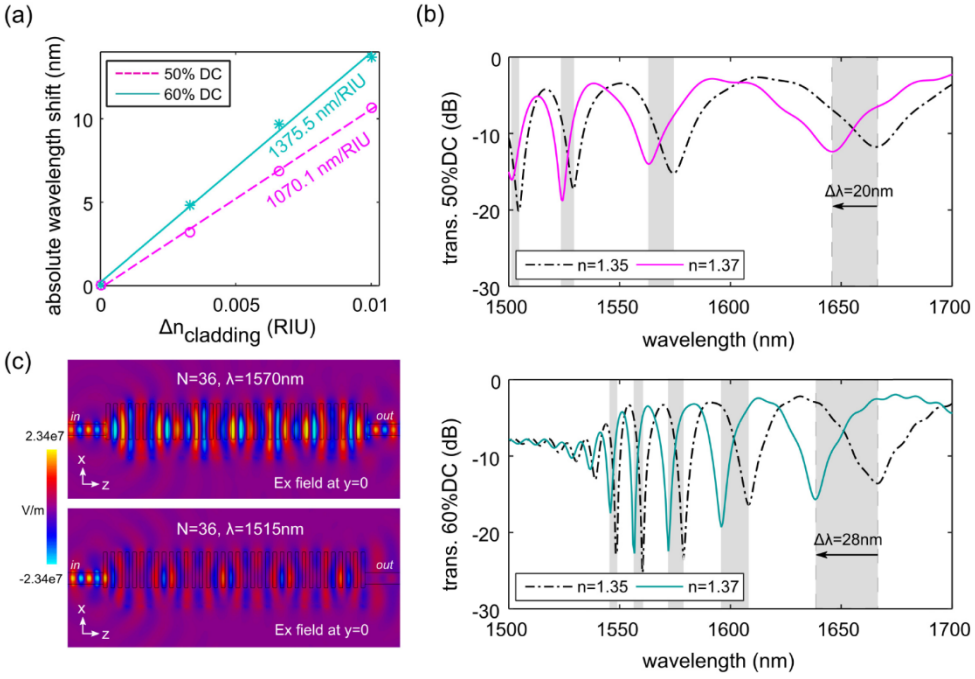

Fig. 6. (a) Spectral shift as a function of cladding RI variations for 50% and 60% duty cycles with N = 120 and N = 220 periods, respectively. Design parameters are Λ = 290nm, w = 1400nm, h = 220nm and d = 375nm with a silica lower cladding and under an aqueous environment of 1.36RIU. (b) Transmission spectra for 50% duty cycle (top) and 60% duty cycle (bottom) at different RI scenarios. The shaded areas represent the spectral shift of the interference fringes for a cladding RI increment from 1.35RIU to 1.37RIU. (c) x-component of the electric field at y = 0 slice, for N = 36 periods and 50%DC. The upper contour map

Optics EXPRESS

represents maximum transmission for a wavelength exhibiting constructive interference. The lower contour map depicts minimum transmission for a wavelength where a spectral dip is located (i.e., destructive interference). Note that for this number of SWG elements N, spectral dips are located at different wavelengths regarding the previous spectrum.

Moreover, the use of two significantly different lengths also allows us to demonstrate that the spectral shift sensitivity is independent of the sensor length, as well as to confirm that a higher number of spectral fringes is obtained for longer structures (see Fig. 6(b)). It should also be noted that deeper dips are achieved for lower wavelengths, indicating that both SWG modes are almost equally excited, while that modal excitation is not as balanced for higher wavelengths and shallower dips are obtained. Additionally, spectral dips are narrower and more grouped for lower wavelengths as a consequence of the dispersion properties of the odd mode at this region. These two factors make that higher quality factors are achieved for the spectral dips located at lower wavelengths. Therefore, although the spectral sensitivity does not directly depend on the coupling ratio between the two modes and on the number of elements N, these are two important parameters to optimize in future experimental developments, since an increase of the quality factor of the spectral dips will allow enhancing the limit of detection of the sensor. On the other hand, we have also to consider that an increase in the number of elements N will be translated into higher propagation losses that could negatively affect the sensor performance. However, as it has been previously explained, the dispersive behavior of the modes propagating in the SWG structure allows to obtain a very high sensitivity without the need of very long lengths, what will also contribute to reducing the insertion losses of the sensor.

Finally, a comparative study between the results obtained in MPB and those from the FDTD simulations is presented in Fig. 7. As it can be observed, both approaches match perfectly: the theoretical semi-analytic study of the sensitivity using Eq. (3) with the dispersion relations calculated using MPB and the shift of the spectral fringes measured when making a FDTD analysis of the complete structure.

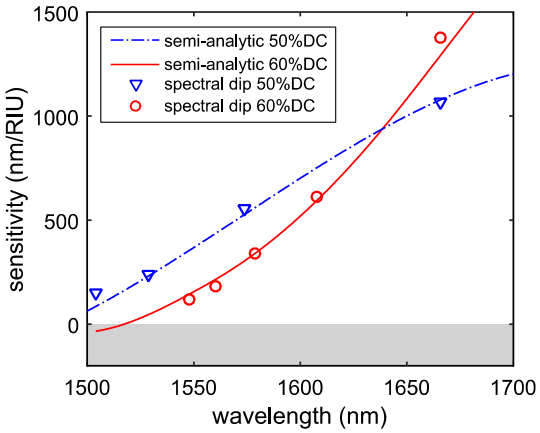

Fig. 7. Comparison between the sensitivity results obtained in MPB and CST for the SWG sensor having a duty cycle of 50% and 60%. Semi-analytical curves (solid and dashed lines) represent the theoretical bulk sensitivity as a function of wavelength obtained using MPB and Eq. (3). Diamonds and circle markers show the sensitivity of certain spectral fringes in the spectrum obtained from the FDTD simulations. The parameters of the SWG sensor are N = 120 for 50%DC, N = 220 for 60%DC, Λ = 290nm, w = 1400nm and h = 220nm in silica lower cladding (n = 1.44) and under an aqueous environment of 1.36RIU. The gray shaded area represents the region where the sign of the spectral sensitivity changes.

5. Conclusions

A new sensor concept including SWG structures and single-channel bimodal interferometers has been presented. The combination of these two concepts allows significantly increasing the

Optics EXPRESS

sensitivity of the device while keeping a compact size. The theoretical background of the SWG bimodal behavior has been studied, as well as its influence in creating critical sensitivity regions in spectral based sensors. A strong dependence with the duty cycle has been determined, since it influences the evolution of the phase shift as a function of wavelength, and thus, the sensitivity. As a result, ultrahigh bulk sensitivity values that can go even above 1300nm/RIU have been obtained both semi-analytically using the dispersion relations of the propagated modes and by means of FDTD simulations. These sensitivity values improve by a factor of 2.5 those reported for SWG RRs, by a factor of almost 6 those reported for conventional RRs and are similar to those reported for other more complex configurations as for the case of slot RRs. Additionally, surface sensitivity has also been studied, obtaining values of up to 6.138nm/nm for 60nm-thick layers, which are, to the best of our knowledge, the highest reported in the literature for integrated photonic sensors on silicon. Furthermore, the SWG bimodal interferometric sensor also presents outstanding surface sensitivity values of more than 2nm/nm for thicknesses of few nanometers, similarly to the best results in SWG RRs.

Funding

European Commission through the Horizon 2020 Programme (PHC-634013 PHOCNOSIS project).

References

1. S. M. Rytov, "Electromagnetic properties of a finely stratified medium," JETP, Sov. Phys. **2**(3), 466–475 (1956).
2. J. Topol'ančik, P. Bhattacharya, J. Sabarinathan, and P. C. Yu, "Fluid detection with photonic crystal-based multichannel waveguides," Appl. Phys. Lett. **82**(8), 1143–1145 (2003).
3. J. D. Joannopoulos, P. R. Villeneuve, and S. Fan, "Photonic crystals: Putting a new twist on light," Nature **386**(6621), 143–149 (1997).
4. M. Soljačić, S. G. Johnson, S. Fan, M. Ibanescu, E. Ippen, and J. D. Joannopoulos, "Photonic-crystal slow-light enhancement of nonlinear phase sensitivity," J. Opt. Soc. Am. B **19**(9), 2052–2059 (2002).
5. M. Povinelli, S. Johnson, and J. Joannopoulos, "Slow-light, band-edge waveguides for tunable time delays," Opt. Express **13**(18), 7145–7159 (2005).
6. E. Chow, A. Grot, L. W. Mirkarimi, M. Sigalas, and G. Girolami, "Ultracompact biochemical sensor built with two-dimensional photonic crystal microcavity," Opt. Lett. **29**(10), 1093–1095 (2004).
7. N. Skivesen, A. Têtu, M. Kristensen, J. Kjems, L. H. Frandsen, and P. I. Borel, "Photonic-crystal waveguide biosensor," Opt. Express **15**(6), 3169–3176 (2007).
8. J. G. Castelló, V. Toccafondo, P. Pérez-Millán, N. S. Losilla, J. L. Cruz, M. V. Andrés, and J. García-Rupérez, "Real-time and low-cost sensing technique based on photonic bandgap structures," Opt. Lett. **36**(14), 2707–2709 (2011).
9. P. Cheben, R. Halir, J. H. Schmid, H. A. Atwater, and D. R. Smith, "Subwavelength integrated photonics," Nature **560**(7720), 565–572 (2018).
10. R. Halir, P. Cheben, J. M. Luque-González, J. D. Sarmiento-Merenguel, J. H. Schmid, G. Wangüemert-Pérez, D. X. Xu, S. Wang, A. Ortega-Moñux, and Í. Molina-Fernández, "Ultra-broadband nanophotonic beamsplitter using an anisotropic sub-wavelength metamaterial," Laser Photonics Rev. **10**(6), 1039–1046 (2016).
11. D. Benedikovic, M. Berciano, C. Alonso-Ramos, X. Le Roux, E. Cassan, D. Marris-Morini, and L. Vivien, "Dispersion control of silicon nanophotonic waveguides using sub-wavelength grating metamaterials in near- and mid-IR wavelengths," Opt. Express **25**(16), 19468–19478 (2017).
12. J. M. Luque-González, A. Herrero-Bermello, A. Ortega-Moñux, Í. Molina-Fernández, A. V. Velasco, P. Cheben, J. H. Schmid, S. Wang, and R. Halir, "Tilted subwavelength gratings: controlling anisotropy in metamaterial nanophotonic waveguides," Opt. Lett. **43**(19), 4691–4694 (2018).
13. J. Flueckiger, S. Schmidt, V. Donzella, A. Sherwali, D. M. Ratner, L. Chrostowski, and K. C. Cheung, "Sub-wavelength grating for enhanced ring resonator biosensor," Opt. Express **24**(14), 15672–15686 (2016).
14. J. Gonzalo Wangüemert-Pérez, P. Cheben, A. Ortega-Moñux, C. Alonso-Ramos, D. Pérez-Galacho, R. Halir, I. Molina-Fernández, D.-X. Xu, and J. H. Schmid, "Evanescent field waveguide sensing with subwavelength grating structures in silicon-on-insulator," Opt. Lett. **39**(15), 4442–4445 (2014).
15. J. G. Wangüemert-Pérez, A. Hadij-ElHouati, A. Sánchez-Postigo, J. Leuermann, D. X. Xu, P. Cheben, A. Ortega-Moñux, R. Halir, and Í. Molina-Fernández, "Subwavelength structures for silicon photonics biosensing," Opt. Laser Technol. **109**, 437–448 (2019).
16. P. Kozma, F. Kehl, E. Ehrentreich-Förster, C. Stamm, and F. F. Bier, "Integrated planar optical waveguide interferometer biosensors: a comparative review," Biosens. Bioelectron. **58**, 287–307 (2014).
17. Q. Liu, X. Tu, K. W. Kim, J. S. Kee, Y. Shin, K. Han, Y. J. Yoon, G. Q. Lo, and M. K. Park, "Highly sensitive Mach-Zehnder interferometer biosensor based on silicon nitride slot waveguide," Sens. Actuators B Chem. **188**,

Optics EXPRESS

681–688 (2013).
18. D. Sarkar, N. S. K. Gunda, I. Jamal, and S. K. Mitra, "Optical biosensors with an integrated Mach-Zehnder Interferometer for detection of Listeria monocytogenes," Biomed. Microdevices **16**(4), 509–520 (2014).
19. R. Levy and S. Ruschin, "Critical sensitivity in hetero-modal interferometric sensor using spectral interrogation," Opt. Express **16**(25), 20516–20521 (2008).
20. R. Levy, S. Ruschin, and D. Goldring, "Critical sensitivity effect in an interferometer sensor," Opt. Lett. **34**(19), 3023–3025 (2009).
21. R. Levy and S. Ruschin, "Design of a single-channel modal interferometer waveguide sensor," IEEE Sens. J. **9**(2), 1 (2009).
22. K. E. Zinoviev, A. B. González-Guerrero, C. Domínguez, and L. M. Lechuga, "Integrated bimodal waveguide interferometric biosensor for label-free analysis," J. Lit. Technol. **29**(13), 1926–1930 (2011).
23. D. Duval, A. B. González-Guerrero, S. Dante, J. Osmond, R. Monge, L. J. Fernández, K. E. Zinoviev, C. Domínguez, and L. M. Lechuga, "Nanophotonic lab-on-a-chip platforms including novel bimodal interferometers, microfluidics and grating couplers," Lab Chip **12**(11), 1987–1994 (2012).
24. C. S. Huertas, D. Fariña, and L. M. Lechuga, "Direct and label-free quantification of micro-RNA-181a at attomolar level in complex media using a nanophotonic biosensor," ACS Sens. **1**(6), 748–756 (2016).
25. C. S. Huertas, S. Domínguez-Zotes, and L. M. Lechuga, "Analysis of alternative splicing events for cancer diagnosis using a multiplexing nanophotonic biosensor," Sci. Rep. **7**(1), 41368 (2017).
26. P. Lalanne and M. Hutley, "Artificial media optical properties – subwavelength scale," Encycl. Opt. Eng. **1**, 62–71 (2003).
27. P. J. Bock, P. Cheben, J. H. Schmid, J. Lapointe, A. Delâge, S. Janz, G. C. Aers, D.-X. Xu, A. Densmore, and T. J. Hall, "Subwavelength grating periodic structures in silicon-on-insulator: a new type of microphotonic waveguide," Opt. Express **18**(19), 20251–20262 (2010).
28. K. De Vos, I. Bartolozzi, E. Schacht, P. Bienstman, and R. Baets, "Silicon-on-Insulator microring resonator for sensitive and label-free biosensing," **15**(12), 7610–7615 (2007).
29. L. Chrostowski, S. Grist, J. Flueckiger, W. Shi, X. Wang, E. Ouellet, H. Yun, M. Webb, B. Nie, Z. Liang, K. C. Cheung, S. A. Schmidt, D. M. Ratner, and N. A. F. Jaeger, "Silicon photonic resonator sensors and devices," Proc. SPIE **8236**, 823620 1–16 (2012).
30. S. Johnson and J. Joannopoulos, "Block-iterative frequency-domain methods for Maxwell's equations in a planewave basis," Opt. Express **8**(3), 173–190 (2001).
31. E. Luan, H. Yun, L. Laplatine, K. Cheung, Y. Dattner, D. Ratner, J. Flückiger, and L. Chrostowski, "Sub-wavelength multi-box waveguide-based label-free sensors," Integr. Opt. Devices, Mater. Technol. XXII **10535**, 105350H (2018).
32. W. Zhang, S. Serna, X. Le Roux, L. Vivien, and E. Cassan, "Highly sensitive refractive index sensing by fast detuning the critical coupling condition of slot waveguide ring resonators," Opt. Lett. **41**(3), 532–535 (2016).
33. A. Fernández Gavela, D. Grajales García, J. C. Ramirez, and L. M. Lechuga, "Last advances in silicon-based optical biosensors," Sensors (Basel) **16**(3), 285 (2016).
34. E. Luan, H. Yun, L. Laplatine, Y. Dattner, D. M. Ratner, K. C. Cheung, and L. Chrostowski, "Enhanced sensitivity of subwavelength multibox waveguide microring resonator label-free biosensors," IEEE J. Sel. Top. Quantum Electron. **25**(3), 1–11 (2019).

158.42.159.77 {ts '2019-03-11 05:18:48'}